Metric-affine gravity effects on terrestrial exoplanet profiles

Aleksander Kozak[1,*] and Aneta Wojnar[2,†]

[1]*Institute of Theoretical Physics, University of Wroclaw, Plac Maxa Borna 9, 50-206 Wroclaw, Poland*
[2]*Laboratory of Theoretical Physics, Institute of Physics, University of Tartu, Wilhelm Ostwaldi 1, 50411 Tartu, Estonia*

(Received 12 July 2021; accepted 24 September 2021; published 27 October 2021)

Mass-radius relations of homogeneous cold spheres are obtained for six solid materials commonly found in terrestrial planets. An additional degeneracy in the (exo)planet profiles is discussed together with their properties concluded from our findings in the framework of Palatini $f(\mathcal{R})$ gravity. Moreover, a new test of gravity has been proposed: The results presented here will allow us to test and constrain models of gravity by the use of seismic data acquired from earthquakes and marsquakes.

DOI: 10.1103/PhysRevD.104.084097

I. INTRODUCTION

General relativity (GR) has been tested experimentally on a number of occasions [1]. Just recently, the existence of one of the most astonishing predictions made by Einstein's theory, black holes, has been confirmed by detecting gravitational waves coming from a merger of two of them [2]. Also, the shadow of a supermassive black hole in the center of M87 galaxy has been recently observed directly [3–6] (see Ref. [7] for a review). Despite all these triumphs, GR cannot account for various cosmological and astrophysical phenomena in a satisfactory way. A lot of effort has been dedicated to constructing alternative models capable of solving the dark matter and dark energy problem [8–13], shedding some light on spacetime singularities [14], or providing unification scenarios at high energies [15,16]. Another problem concerns the observed maximum masses of compact objects that exceed theoretical predictions [17–20] and the mass of a binary black hole merger [21,22].

In this work, we use the fact that many models of gravitation—in particular, $f(\mathcal{R})$ Palatini gravity (see Sec. II for a short review of the model)—slightly alter the nonrelativistic limit of (sub)stellar structural equations by introducing new (geometric) terms proportional to functions of energy density [23–25] (for a review, see Refs. [26,27]). Modified nonrelativistic equations in the context of stars and brown dwarfs have already been widely used by the physics community, mainly to obtain limiting masses, such as, e.g., the Chandrasekhar mass for white dwarf stars [28–33], the minimum Main Sequence mass[1] [34–37], or the minimum mass for deuterium burning [38]. Moreover, modified gravity also impacts the early evolution of low-mass stars [39], the post–Main Sequence stage of population II stars [40], and the cooling processes of brown dwarfs [41], as well as altering the age-estimation procedures based on the lithium depletion method [42].

Therefore, using modified equations describing a spheri cal-symmetric object, we reveal an additional degeneracy induced by metric-affine gravity in the mass-radius relations for a cold homogeneous sphere. Such an object can be treated as a single-layer (exo)planet, and it is useful to demonstrate that the modified gravity effects also take part in the planetary description. To show that, we use equations of state in analytical form for six solid materials, and modified hydrostatic equilibrium equations presented in Sec. III and the Appendix. We also discuss a possible singularity caused by a particular combination of an equation of state and the theory parameter, and we argue that for a physical system such as a star or a planet, this problem will not appear. In Sec. IV, we numerically solve the equations and demonstrate the mass-radius relations and density profiles obtained for the Palatini quadratic model. Section V is devoted to a description of a new test of gravity with the use of our results and seismic data from earthquakes and marsquakes. In the last section, we draw our conclusions.

Let us notice that so far, (exo)planets have been used to test and constrain theories of gravity only in the context of precessions of planetary perihelion in the Solar System —see, e.g., Refs. [43–54], and modifications to Kepler's third law by introducing corrections to Kepler's third law [55,56].

We use $(-+++)$ signature convention and $\kappa^2 = 8\pi G/c^4$.

*aleksander.kozak@uwr.edu.pl
†aneta.magdalena.wojnar@ut.ee

[1]That is, a star reaches the Main Sequence when the energy produced in the star's core by hydrogen burning is balancing the gravitational contraction.

II. PALATINI $f(\mathcal{R})$ GRAVITY

In the metric approach to $f(R)$ gravity, where one replaces the Einstein-Hilbert Lagrangian with a general function of the curvature scalar, a metric tensor is the only object mediating the gravitational interaction. It is possible, however, to introduce an independent connection and split up spacetime structure into metric and affine components. Such an approach is called "Palatini," and it exhibits some advantages over the metric formulations [57–60].

The action is given by

$$S[g,\Gamma,\psi_m]=\frac{1}{2\kappa^2}\int\sqrt{-g}f(\mathcal{R})d^4x+S_{\text{matter}}[g,\psi_m], \tag{1}$$

where $\mathcal{R}=g^{\mu\nu}\mathcal{R}_{\mu\nu}(\Gamma)$ is the Palatini curvature scalar, built from both the metric and the independent connections, and ψ_m represents the matter fields.

Varying the action with respect to the metric tensor yields

$$f'(\mathcal{R})\mathcal{R}_{\mu\nu}-\frac{1}{2}f(\mathcal{R})g_{\mu\nu}=\kappa^2T_{\mu\nu}, \tag{2}$$

with $T_{\mu\nu}=-\frac{2}{\sqrt{-g}}\frac{\delta S_m}{\delta g_{\mu\nu}}$ and the prime denoting differentiation with respect to the curvature. One can contract Eq. (2) with the metric and relate the Palatini curvature to the trace of the energy-momentum tensor:

$$f'(\mathcal{R})\mathcal{R}-2f(\mathcal{R})=\kappa^2T. \tag{3}$$

We immediately notice that the relation between the curvature and the trace becomes purely algebraic, which means that, for a particular choice of the function f, it is possible to solve it.

In order to obtain the relation between the connection and the metric tensor, one needs to vary with respect to it and obtain the following:

$$\nabla_\beta(\sqrt{-g}f'(\mathcal{R}(T))g^{\mu\nu})=0, \tag{4}$$

where the covariant derivative is defined using the independent connection. If one defines a new metric tensor, conformally related to $g_{\mu\nu}$,

$$h_{\mu\nu}=f'(\mathcal{R}(T))g_{\mu\nu} \tag{5}$$

then Eq. (4) can be written as

$$\nabla_\beta(\sqrt{-h}h^{\mu\nu})=0, \tag{6}$$

and by a well-known theorem, this means that the connection $\Gamma^\alpha_{\mu\nu}$ is Levi-Civita with respect to the metric $h_{\mu\nu}$ [61–63]. Therefore, the "independent" connection turns out to be an auxiliary field and can be integrated out. All relevant degrees of freedom are related to the metric tensor.

Just like its metric counterpart, Palatini $f(\mathcal{R})$ has a scalar-tensor representation, which can be obtained by means of the Legendre transformation:

$$S[g,\Phi,\Gamma,\psi_m]=\frac{1}{2\kappa^2}\int\sqrt{-g}[\Phi\mathcal{R}-V(\Phi)]d^4x+S_{\text{matter}}[g,\psi_m], \tag{7}$$

where $\Phi=df/dR$ and $V(\Phi)=f'(\mathcal{R}(\Phi))\mathcal{R}(\Phi)-f(\mathcal{R}(\Phi))$. It can significantly simplify the problems analyzed [64–68]. The connection, building the Ricci tensor, can be expressed in terms of the scalar field Φ and the metric tensor $g_{\mu\nu}$, yielding

$$S[g,\Phi,\psi_m]=\frac{1}{2\kappa^2}\int\sqrt{-g}\left[\Phi R+\frac{3}{2\Phi}(\partial\Phi)^2-V(\Phi)\right]d^4x+S_{\text{matter}}[g,\psi_m], \tag{8}$$

which is, effectively, a fully metric theory.

Palatini $f(\mathcal{R})$ theory is a special case of a more general class of modified gravity, represented by the following action functional:

$$S[g,\Phi,\Gamma,\psi_m]=\frac{1}{2\kappa^2}\int\sqrt{-g}[\mathcal{A}(\Phi)R(g,\Gamma)-\mathcal{B}(\Phi)(\partial\Phi)^2-\mathcal{V}(\Phi)]d^4x+S_{\text{matter}}[e^{2\alpha(\Phi)}g,\psi_m]. \tag{9}$$

Here, in order to keep the considerations at the most general level possible, we do not specify if the curvature is fully metric, or constructed *à la* Palatini. As one can see, there are four functions of the scalar field entering the action. When specifying the functions, one gets a particular scalar-tensor theory. By means of field equations, one can establish an equivalence between Palatini and metric approaches to this class of modified gravity; such representations will have different values of the scalar field functions.

By comparing Eqs. (7) and (9), one can identify the functions defining general Palatini $f(R)$ gravity in the metric scalar-tensor representation:

$$\mathcal{A}(\Phi)=\Phi,\qquad \mathcal{B}(\Phi)=-\frac{3}{2\Phi},\qquad \mathcal{V}(\Phi)=V(\Phi),\qquad \alpha(\Phi)=0. \tag{10}$$

[The potential $V(\Phi)$ was introduced in Eq. (7).] Since the potential is the only unspecified function of the scalar field, all the information about the f function will be stored therein.

For any scalar-tensor theory, either in the metric, or in the Palatini formalism, one can introduce quantities whose values remain the same under a Weyl (or conformal) transformation of the metric tensor and a reparametrization of the scalar field, defined by Refs. [69–75]

$$\begin{cases} \bar{g}_{\mu\nu} = e^{2\gamma(\Phi)} g_{\mu\nu} \\ \bar{\Phi} = \bar{f}(\Phi) \end{cases}, \tag{11}$$

where $\gamma(\Phi)$ is some function of the scalar field. Performing a conformal change might be treated as a mathematical tool allowing one to choose a set of scalar field functions, for which solving field equations will be particularly simple; expressing relevant quantities in terms of invariants might provide a framework for the analysis of different approaches and theories within one framework.

The invariants used in this work are defined as follows:

$$\mathcal{I}_1(\Phi) = \frac{\mathcal{A}(\Phi)}{e^{2\alpha(\Phi)}}, \tag{12}$$

$$\mathcal{I}_2(\Phi) = \frac{\mathcal{V}(\Phi)}{\mathcal{A}^2(\Phi)}, \tag{13}$$

$$\frac{d\mathcal{I}}{d\Phi} = \sqrt{\frac{\mathcal{B}}{\mathcal{A}} + \delta_\Gamma \left(\frac{3\mathcal{A}'}{2\mathcal{A}}\right)^2}, \tag{14}$$

where δ_Γ is 1 for metric theory, and 0 for Palatini. The prime denotes differentiation with respect to the scalar field.

As one can see, the invariants are functions of the scalar field in the most general case. The Palatini $f(R)$ is somewhat special in this regard, since the scalar field is nondynamical and can be algebraically related to the trace of the energy-momentum tensor. To see this, let us notice that varying Eq. (7) with respect to the scalar field gives

$$\mathcal{R} - V'(\Phi) = 0, \tag{15}$$

which then can be used in Eq. (3) to relate Φ and T. For perfect fluid, $T = -c^2\rho + 3p$, and therefore all invariants can be shown as functions of the trace:

$$\mathcal{I}_i(\Phi(T)) = \mathcal{I}_i(-c^2\rho + 3p), \tag{16}$$

as soon will be demonstrated [cf. Eq. (23)].

III. PALATINI PLANETS

A. Equations of state for cold low-mass spheres

In the following work, we will use equations of states (EOSs) for six different solid materials (see Tables I and II). The first one concerns a case with the assumption of uniform or zero temperature, with pressures below 200 GPa. For such conditions, we are equipped with the analytical form of the EOS given by the fits to the experimental data:

$$p = \frac{3}{2} K_0 (\eta^{7/3} - \eta^{5/3}) \left(1 + \frac{3}{4}(K_0' - 4)(\eta^{2/3} - 1)\right), \tag{17}$$

where $\eta = \rho/\rho_0$ is the compression ratio with respect to the ambient density ρ_0 (that is, the density at zero pressure), and $K_0 = -V(\partial p/\partial V)_T$ is the bulk modulus of the material (the inverse of the compressibility) [76], while K_0' and K_0'' are the first and second pressure derivatives, respectively. Since most of the experiments are limited to $p < 150$ GPa and temperatures less than 2000 K, we will take that as the starting value at the core of the planet. The above EOS is called the third-order finite strain Birch-Murgnagham equation of state (BME) [77,78]. In Table I, there are only two materials which we are using in this work—see our discussion in Sec. IV; for more fits for various materials, see, e.g., Refs. [78,79].

For $p \gtrsim 10^4$ GPa, the electron degeneracy becomes important. The common approach is to match Eq. (17) with the Thomas-Fermi-Dirac equation of state (TFD EOS) [80–83] with a density-dependent correlation energy term added [84] in order to take into account interactions between electrons themselves, obeying the Pauli exclusion principle and moving in the Coulomb field of the nuclei. However, it turns out that the merger of the BME and TFD equations of state can be approximated by a modified polytropic equation of state [79], called the Seager-Kuchner-Hier-Majumder-Militzer equation of state (SKHM EOS),

$$\rho(p) = \rho_0 + c p^n, \tag{18}$$

whose best-fit parameters ρ_0, c, and n are given in Table II. The reason for such a modification, given here by the added ρ_0, is to include the incompressibility of solids and liquids at low pressures. Equation (18) with the given fits for the considered solid materials is valid for the pressure range $p < 10^7$ GPa.

TABLE I. Best-fit parameters for the BME [Eq. (17)]; for more materials, see, e.g., Table 4.1 in Ref. [78] and Table 1 in Ref. [79].

Material	ρ_0 (Mg m^{-3})	K_0 (GPa)	K_0'
Fe(α)	7.86	162.5	5.5
(Mg, Fe)SiO_3	4.26	266	3.9

TABLE II. Best-fit parameters for the SKHM EOS [Eq. (18)] obtained in Ref. [79].

Material	ρ_0 (kg m^{-3})	c (kg m^{-3} Pa^{-n})	n
Fe(α)	8300	0.00349	0.528
$MgSiO_3$	4100	0.00161	0.541
(Mg, Fe)SiO_3	4260	0.00127	0.549
H_2O (ice)	1460	0.00311	0.513
C (graphite)	2250	0.00350	0.514
SiC	3220	0.00172	0.537

B. General structural equations

It was shown that the full relativistic hydrostatic equilibrium equation for the quadratic model in Palatini $f(\mathcal{R})$ gravity,

$$f(\mathcal{R}) = \mathcal{R} + \beta\mathcal{R}^2,$$

is given by Refs. [24,68]:

$$p' = \left[-\frac{G\mathcal{M}(r)}{c^2 r^2 \mathcal{I}_1^{1/2}}(c^2\rho + p)\left(1 - \frac{2G\mathcal{M}(r)}{c^2 r \mathcal{I}_1^{1/2}}\right)^{-1} \times \left(1 + \frac{4\pi \mathcal{I}_1^{\frac{3}{2}} r^3}{c^2 \mathcal{M}(r)}\left(\frac{p}{\mathcal{I}_1^2} + \frac{\mathcal{I}_2}{2\kappa^2}\right)\right)\right] \times \left(\frac{r}{2}\partial_r \ln \mathcal{I}_1 + 1\right) + (-c^2\rho + 5p)\partial_r \ln \mathcal{I}_1. \quad (19)$$

As was already mentioned, the invariants now are functions of the trace of the energy-momentum tensor, since, for the quadratic model,

$$1 + 2\beta\mathcal{R} = \Phi, \quad (20)$$

so that Eq. (3) becomes

$$\frac{-\Phi + 1}{4\beta} = \kappa^2 T, \quad (21)$$

allowing one to write

$$\Phi = 1 - 4\beta\kappa^2(-c^2\rho + 3p). \quad (22)$$

Then, one gets:

$$\mathcal{I}_1 = \Phi = 1 + 4\beta\kappa^2(c^2\rho - 3p), \quad (23)$$

$$\mathcal{I}_2 = \frac{(\Phi - 1)^2}{4\beta\Phi^2} = \frac{4\beta\kappa^4(c^2\rho - 3p)^2}{(1 + 4\beta\kappa^2(c^2\rho - 3p))^2}, \quad (24)$$

where the prime denotes a derivative with respect to the r coordinate. The mass function, after applying the above forms of the invariants, is

$$\mathcal{M}(r) = \int_0^r 4\pi\tilde{r}^2 \frac{\rho - 2c^{-2}\beta\kappa^2(c^2\rho - 3p)^2}{(1 + 4\beta\kappa^2(c^2\rho - 3p))^{1/2}} \times \left[1 + \frac{\tilde{r}}{2}\partial_{\tilde{r}} \ln\left(1 + 4\beta\kappa^2(c^2\rho - 3p)\right)\right] d\tilde{r}. \quad (25)$$

This formula expresses the fact that, in modified gravity theories, the mass function is also altered. One would assume that the total mass should be obtained by integrating the density over a sufficiently large region of space. In the case of GR, the procedure assumes integrating from $r = 0$ to $r = R_S$, where R_S is the radius of the compact object. Metric $f(R)$ gravity predicts, however, that there will be differences between the mass enclosed in a sphere of radius R_S and that measured by a distant observer (at $r = \infty$), since the mass formula includes additional terms coming from modification of the theory [85]. This fact alone shows that one must carefully specify what mass definition one is using. In the present paper, we focus on masses contained within a sphere of radius $r = R_S$, as the effect of a gravisphere is not present in Palatini $f(R)$ gravity, since in the vacuum all contributions from energy density and pressure vanish. However, the theory does introduce extra terms in the interior solutions which carry information about the gravitational energy of the system [86]. We have compared the modified mass function [Eq. (25)] with the usual one for the low-mass cases discussed in the paper, which results in a conclusion that the effect of additional terms in Eq. (25) is minuscule, as presented in Fig. 1. The situation can differ in the case of compact objects, though, and should be carefully studied.

Let us notice that the above equations are exact—that is, no approximation has been applied yet. In what follows, we will use a redefined Starobinsky parameter:

$$\alpha := 2c^2\kappa^2\beta. \quad (26)$$

It should be commented that this defined parameter has a very small value compared to the Starobinsky parameter β, whose value must be large in order to take into account the higher-curvature term, given here by $\mathcal{R}^2$.

Since the conformal transformation (given by the invariant $\mathcal{I}_1$ in our model) was used in order to get the equations written with respect to the physical quantities, the mass and hydrostatic equilibrium equations are singular for a particular value of the parameter α, which depends on energy density and pressure:

$$\alpha_{\text{sing}} = -\frac{1}{2(\rho - \frac{3p}{c^2})}. \quad (27)$$

A possible singular behavior of the additional terms in TOV equations provided by particular equations of state in different models of gravity has been already detected in previous works [87–92]. Such a feature arises from the fact that the modifications often provide new matter-dependent contributions to the hydrostatic equilibrium equation and stability conditions [39,68], via algebraic relation between scalar curvature and matter, as happens in models of metric-affine gravity considered here, or a modified Klein-Gordon equation, relating the dynamics of the scalar field[2] with the ordinary matter sources.

Moreover, it should be taken into account that the singular value of the parameter changes with the energy

[2]This is an extra degree of freedom in a given scalar-tensor theory.

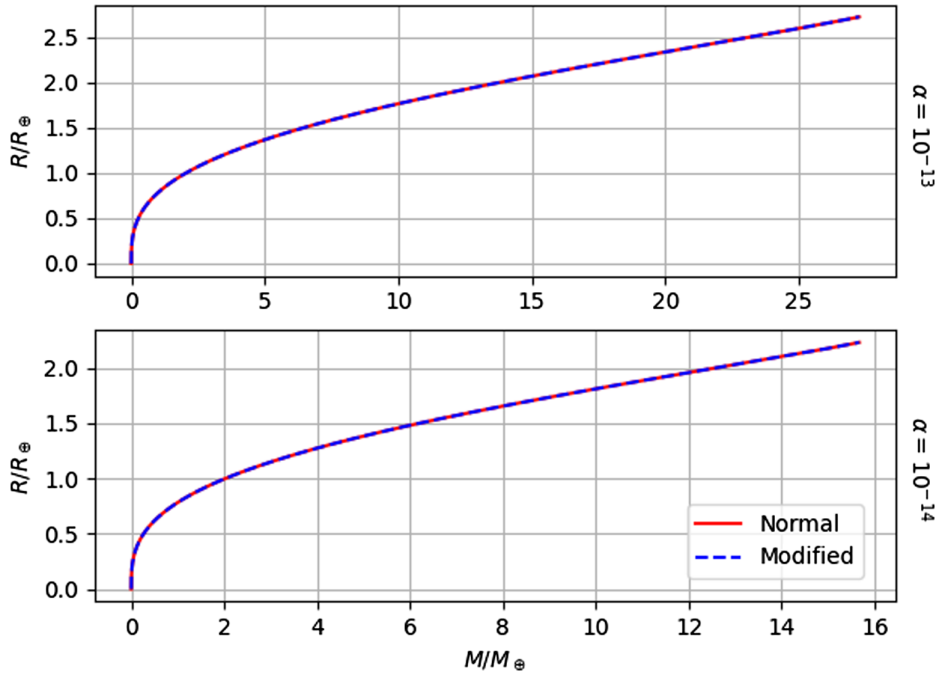

FIG. 1. Mass as a function of the radius of a spherically symmetric object composed of $(\mathrm{Mg,Fe})\mathrm{Sio}_3$ in Palatini theory for two different values of the parameter α. The red curve represents mass computed by integrating the standard equation $\mathcal{M}' = 4\pi r^2\rho$, whereas the blue dashed line was calculated using Eq. (25). As is clear from the plot, these two curves overlap; numerical results differ by one part in 10^9, which is roughly 4–5 orders of magnitude greater than the parameter α.

density and pressure, according to their profiles—that is, it will have much a smaller value in the core than near the object's surface. Therefore, one should always be very careful when choosing a particular negative value of the parameter α, taking into account the given equation of state and the range of densities/pressures through an examined object. In our case, we are not even close to the singular value, as we would have to consider densities much higher than the ones present in the planetary interiors (and together with the considered EOSs describing planetary compositions) in order to have parameter values that make the equations singular.

C. Structural equation for terrestrial planets

Since we are dealing with planets, the terms proportional to p/c^2 are negligible when compared to the energy density, and hence Eq. (19) reduces to

$$p' = -\frac{G\mathcal{M}\rho}{r^2\mathcal{I}_1^{1/2}}\left(1-\frac{2G\mathcal{M}}{c^2 r\mathcal{I}_1^{1/2}}\right)^{-1} \times\left(1+\frac{4\pi\mathcal{I}_1^{\frac{3}{2}}r^3}{c^2\mathcal{M}}\frac{\mathcal{I}_2}{2\kappa^2}\right)\left(\frac{r}{2}\partial_r\ln\mathcal{I}_1+1\right) - c^2\rho\partial_r\ln\mathcal{I}_1, \tag{28}$$

with

$$\mathcal{I}_1 = 1+2\alpha\rho, \qquad \mathcal{I}_2 = \frac{2\alpha\kappa^2c^2\rho^2}{(1+2\alpha\rho)^2}.$$

The nonrelativistic mass is then

$$\mathcal{M}(r) = \int_0^r 4\pi\tilde{r}^2\frac{\rho-\alpha\rho^2}{(1+2\alpha\rho)^{1/2}} \times\left[1+\frac{\tilde{r}}{2}\partial_{\tilde{r}}\ln(1+2\alpha\rho)\right]d\tilde{r}, \tag{29}$$

while the singular value of the parameter α can be approximated as

$$\alpha_{\mathrm{sing}} = -\frac{1}{2\rho}. \tag{30}$$

This is not the common nonrelativistic limit (we have just neglected the pressure p contribution); the geometric term as well as the gravitational pressure contribution coming from the invariants $\mathcal{I}_1$ and $\mathcal{I}_2$ are still present. The reason for this is that when one expands the equations around $\alpha = 0$, which as we discussed, will be a very small value in our case, one loses the discussed information about the singular behavior of the equations related to the particular value(s) of the parameter, and moreover, as we have checked (see the discussion and equations in the Appendix), the nonphysical profiles occur for the positive α in the case of large planets. Because of that fact, we will use the above equations in order

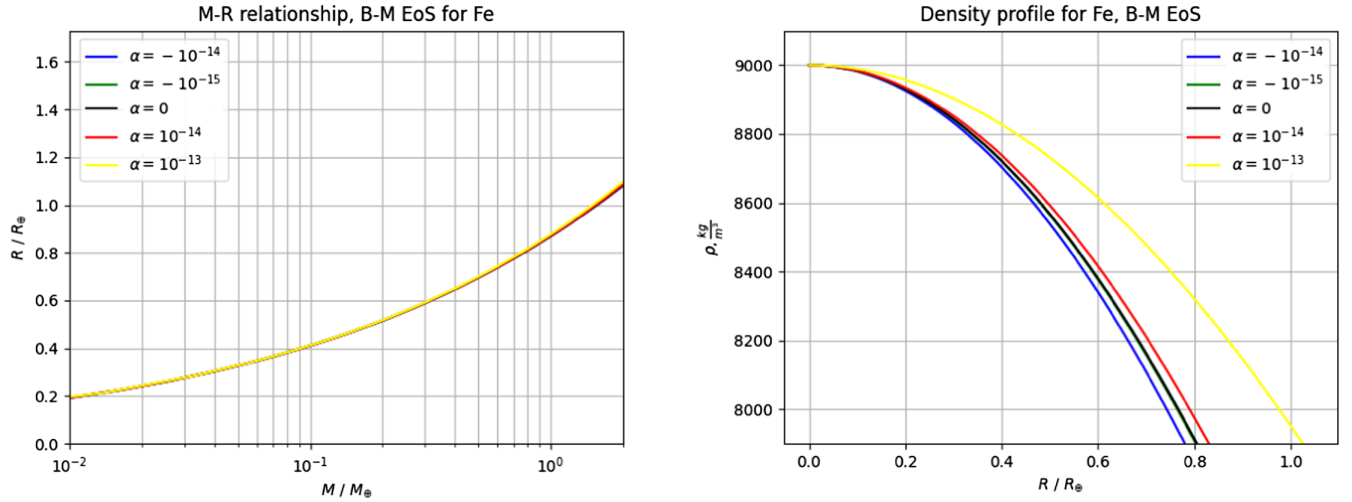

FIG. 2. Mass-radius relation and density profile plots for homogeneous cold spheres of iron for different values of the parameter α ($\alpha = 0$ gives a GR/Newtonian planet), obtained from the Birch-Murgnagham equation of state with the use of the modified hydrostatic equilibrium equations.

to include planets with larger masses—that is, to allow the planets to reach the mass limit when the electron degeneracy must be taken into account.

The structural equations used in the numerical analysis described in Sec. IV are given in the Appendix.

IV. PLANET PROFILES AND NUMERICS

In order to obtain a mass-radius relationship for planets, we integrate Eq. (28) and the mass relation of Eq. (25) (expressed as a derivative). The additional information, allowing one to relate energy density and pressure, is provided by a suitable equation of state. The exact form of the equations used for the case of a polytropic equation of state can be found in the Appendix.

For a given value of the parameter α, the equations were integrated using the fourth-order Runge-Kutta method. The initial conditions at $R = 0$ were $\mathcal{M}(0) = 0$ and $\rho(0) = \rho_c > \rho_0$, and the integration has been carried out for a wide range of possible central densities, starting from a little above ρ_0 for a given material, and finishing at the point where electron degeneracy must be taken into account. The process of integrating for a particular value of ρ_c ends when the density drops to its ambient value—i.e., ρ_0. At this moment, the final mass and radius are read off, and a single point is placed in the mass-radius diagram. After obtaining all relevant data, we change the value of α and repeat the procedure.

A. The Birch-Murgnagham equation of state

Using the BME [Eq. (17)] applied to the hydrostatic equilibrium and mass equations [Eqs. (19) and (25), respectively], one obtains the radius-mass curves and density profiles with respect to each material. Since this EOS is suitable only for the low-pressure regime, the maximal masses should not cross that of the Earth, and even the Earth's core ($p = 364$ GPa according to the PREM model [93]) should not be modeled by it. Therefore, the curves just before reaching the Earth's mass are extrapolated, and they do not describe a realistic mass-radius relation for Earth-sized and larger planets.

Our analysis demonstrates in the mass-radius plots that the Newtonian and modified gravity curves of the homogeneous cold spheres overlap. Because of that fact, we plot only the iron and silicate curves (see Figs. 2 and 3), which are the main abundant materials of the rocky planets in our Solar System. But let us notice that the density profiles do differ even for very small masses ($\alpha = 0$—that is, the GR/Newtonian case—is given by the black curve), making it possible to use this feature to constrain theories of gravity. We discuss this finding in detail in Sec. V.

However, as will be seen in the next subsection, for terrestrial planets with masses and radii bigger than those in the Solar System, we will deal with an extra degeneracy in the radius-mass relations provided by modified gravity.

B. The SKHM (modified polytropic) equation of state

Since the BME [Eq. (17)] does not reproduce reliable results even for the innermost layers of the Earth, we will focus now on the modified polytropic EOS [Eq. (18)], which takes into account the electron degeneracy and interactions between electrons, as well as the particles' motion in the Coulomb field of the nuclei. Such an EOS can be used for the pressure range $p < 10^7$ GPa; therefore, it is our maximal central value in the numerical approach, expressed by ρ_c obtained from Eq. (18).

Our results are given by the plots in Figs. 4–9—that is, mass-radius relations and density profiles for the six most common solid materials found in rocky planets: iron, water

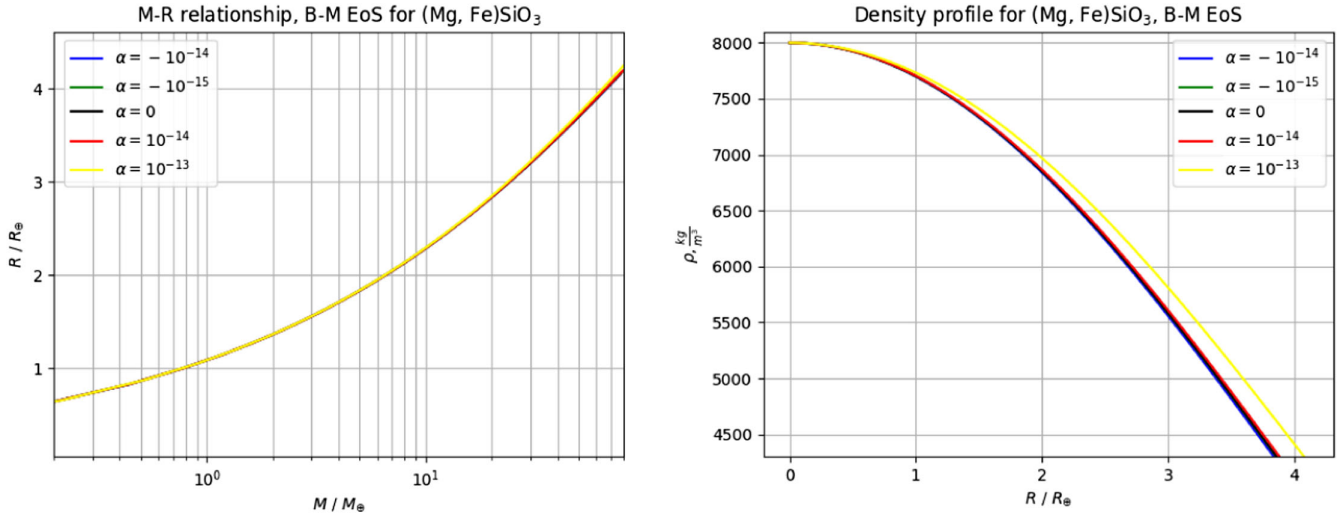

FIG. 3. Mass-radius relation and density profile plots for homogeneous cold spheres of silicate $(\mathrm{Mg,Fe})\mathrm{SiO}_3$ for different values of the parameter α ($\alpha = 0$ gives a GR/Newtonian planet), obtained from the Birch-Murgnagham equation of state with the use of the modified hydrostatic equilibrium equations.

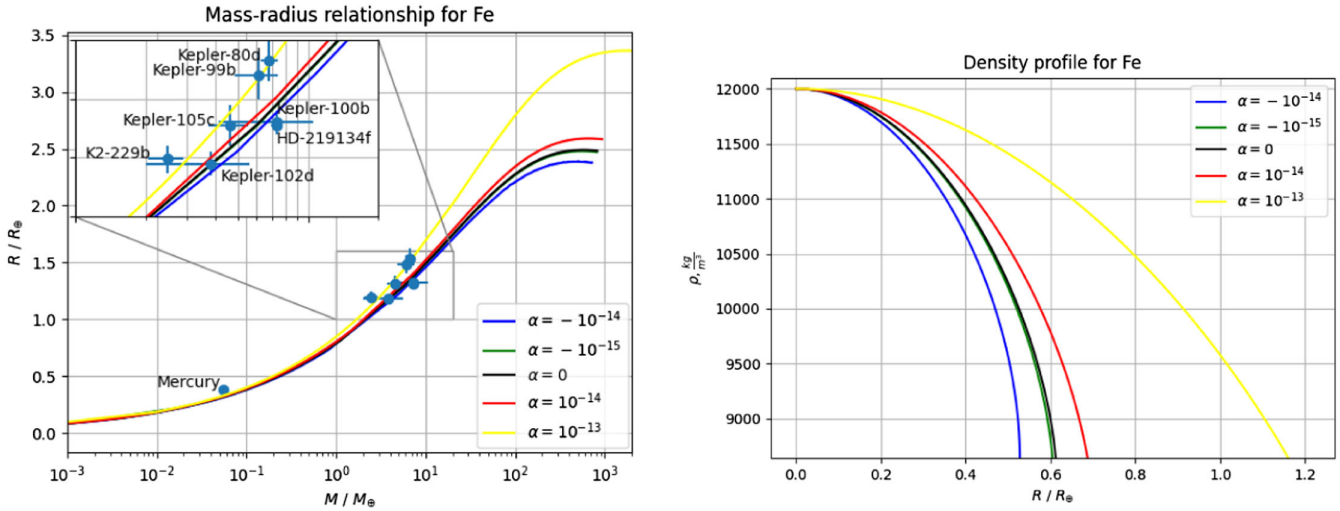

FIG. 4. Mass-radius relation and density profile plots for homogeneous cold spheres of iron for different values of the parameter α (where $\alpha = 0$ gives a GR/Newtonian planet), obtained from the SKHM equation of state with the use of the modified hydrostatic equilibrium equations. Mercury and a few super-Mercury exoplanets are depicted [95,96].

ice, two varieties of silicate, silicon carbide, and graphite. Black curves ($\alpha = 0$) represent the GR/Newtonian case. The curves' flattening on the mass-radius plots in Figs. 4–9, related to the constant planets' radii and even decreasing their values for larger masses, occurs because of electron degeneracy, whose pressure becomes important at high mass (see the discussion in Ref. [94]).

We have also designated the positions on the figures for four rocky (Earth, Venus, Mars, and Mercury) and two ice-giant planets (Uranus and Neptune) of the Solar System, as well as a few exoplanets: super-Mercuries [95,96] on the iron curves (Fig. 4) and super-Earths [96–98] on the silicate curves (Figs. 6 and 7). As we observe, the Earth-like planets can be found along the silicate curves, while Mercury-like ones are found along the iron curves, because those materials are the most abundant in their interiors. Uranus and Neptune are situated significantly above the water-ice curves[3] because of their high abundances of helium, which cannot be modeled by the equations of state used in this work [79,94]. Although our studies are related to toy-model planets—that is, we consider only homogeneous planets without taking into account multiple layers of different compositions—the most important result obtained via this analysis is an additional

[3]They are found between the water-ice and the helium curves, though the latter is not depicted here.

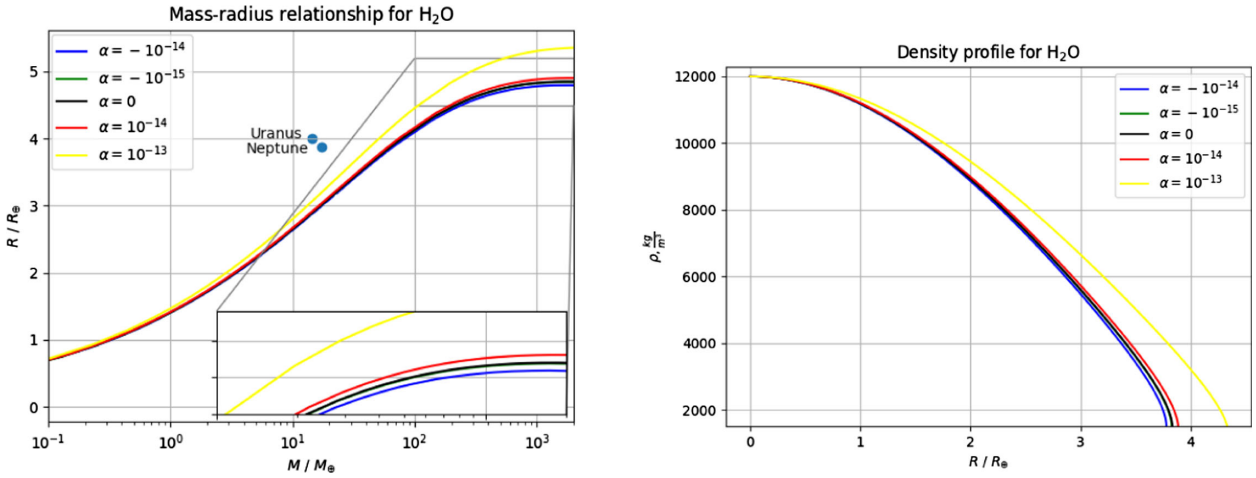

FIG. 5. Mass-radius relation and density profile plots for homogeneous cold spheres of water ice for different values of the parameter α (where $\alpha = 0$ gives a GR/Newtonian planet), obtained from the SKHM equation of state with the use of the modified hydrostatic equilibrium equations. Uranus and Neptune, the giant ice planets, are depicted.

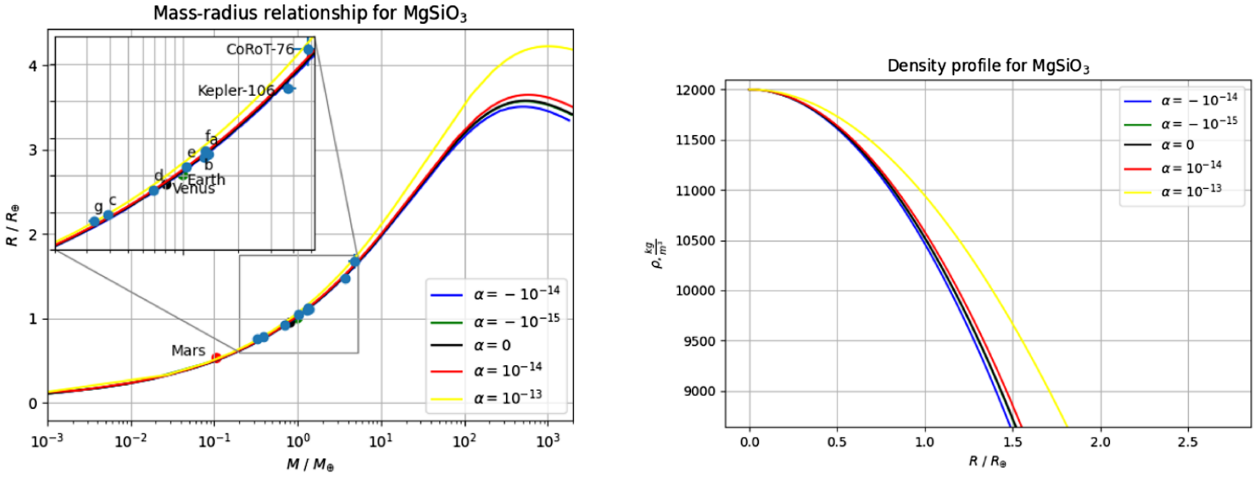

FIG. 6. Mass-radius relation and density profile plots for homogeneous cold spheres of silicate $MgSiO_3$ for different values of the parameter α (where $\alpha = 0$ gives a GR/Newtonian planet), obtained from the SKHM equation of state with the use of the modified hydrostatic equilibrium equations. Mars, Venus, and the Earth, as well as a few terrestrial exoplanets, are depicted [96–98]. The letters denote TRAPPIST-1 planets, whose physical parameters can be found in Ref. [98].

degeneracy in the mass-radius relations caused by modified gravity models. In the GR/Newtonian case, when one deals with a planet having multiple layers of varied compositions, different mass fractions of, for instance, iron cores and silicate mantles can provide the same total radius for a transiting planet of the same mass [79]. Apart from this, we have demonstrated that a similar degeneracy will appear when one applies modified structural equations. A curve of a given material obtained from a model different from the GR/Newtonian gravity model is shifted with respect to the GR/Newtonian curve, and it can overlap with a mixture of two or more materials whose curve was plotted using GR/Newtonian equations.

Moreover, let us notice that, even for the Birch-Murgnagham EOS considered in the above subsection, we are dealing with a notable difference between GR/Newtonian curves and modified gravity curves for the density profiles. That fact can be used to test and to constrain models of gravity when we are equipped with seismic data coming from earthquakes and marsquakes—see the discussion in the next section.

V. A NEW TEST FOR MODELS OF GRAVITY

As clearly demonstrated, although in the case of the simplified modeling of a planet as a single-material sphere, modified gravity affects the internal structure and density profile of such an object. This fact immediately equips us with the possibility to test models of gravity when the internal structure of the planet is well known.

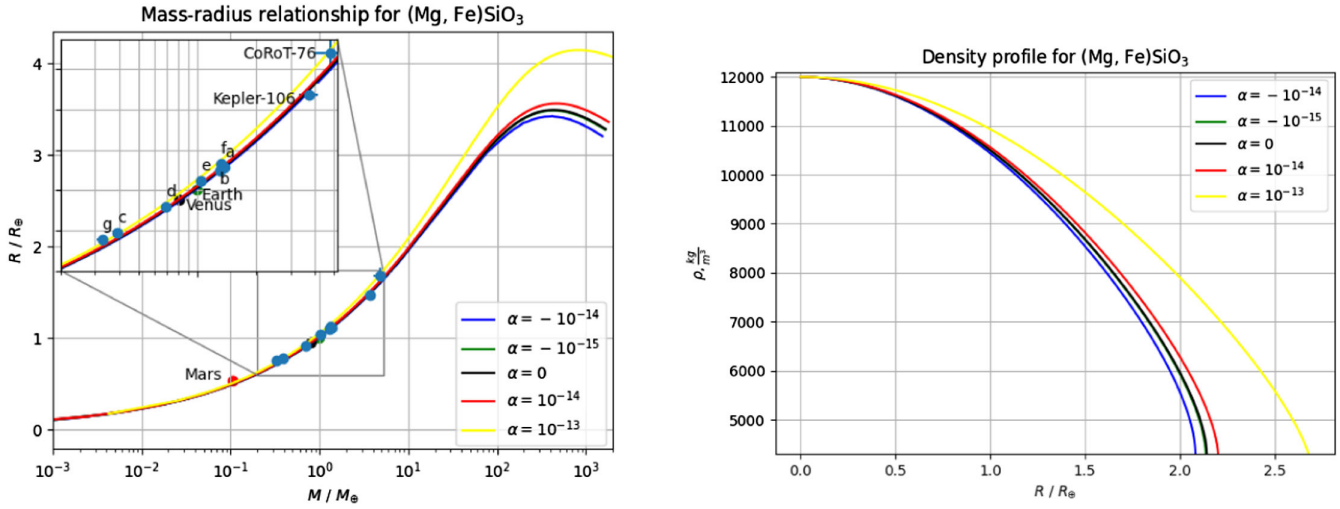

FIG. 7. Mass-radius relation and density profile plots for homogeneous cold spheres of silicate $(\mathrm{Mg,Fe})\mathrm{SiO}_3$ for different values of the parameter α (where $\alpha = 0$ gives a GR/Newtonian planet), obtained from the SKHM equation of state with the use of the modified hydrostatic equilibrium equations. Mars, Venus, and the Earth, as well as a few terrestrial exoplanets, are depicted [96–98]. The letters denote TRAPPIST-1 planets, whose physical parameters can be found in Ref. [98].

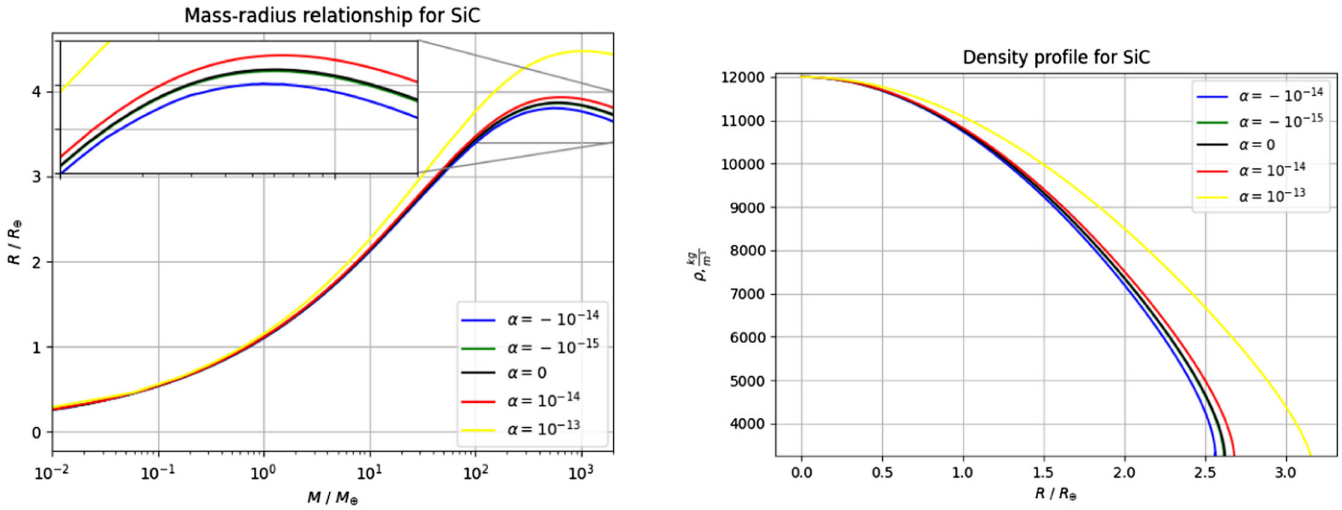

FIG. 8. Mass-radius relation and density profile plots for homogeneous cold spheres of silicon carbide for different values of the parameter α (where $\alpha = 0$ gives a GR/Newtonian planet), obtained from the SKHM equation of state with the use of the modified hydrostatic equilibrium equations.

When the planet's density profile $\rho(r)$ is given, the polar moment of inertia $\mathcal{C}$ can be obtained by the expression

$$\mathcal{C} = \frac{8\pi}{3}\int_0^R \rho(r) r^4 dr, \tag{31}$$

where R is the planet's radius. Roughly speaking, knowing a planet's profile means that the number of differently composed layers and their boundaries are provided. So far, the best-known planet's inner structure is that of the Earth, endowed by the PREM model [93] and its further improvements [99–101] (see more models at Ref. [102]), whereas we will be soon equipped with the Mars model given by the Seismic Experiment for Interior Structure (SEIS)—that is, from NASA's MARS InSight Mission's seismometer [103].

A seismic wave changes when it travels through different layers of the planet. These changes depend on the material that the layer is made of, allowing us to describe the material's characteristics, such as, for example, bulk modulus K_0 (incompressibility), which appears in the EOS [Eq. (17)] via the velocities of the longitudinal and transverse elastic waves, or via the seismic parameter [78].

These density profiles, given by the PREM model and its improvements, assume Newtonian gravity. However, as revealed in our simplified case, the density profiles are also affected by the model of gravity, giving slightly different

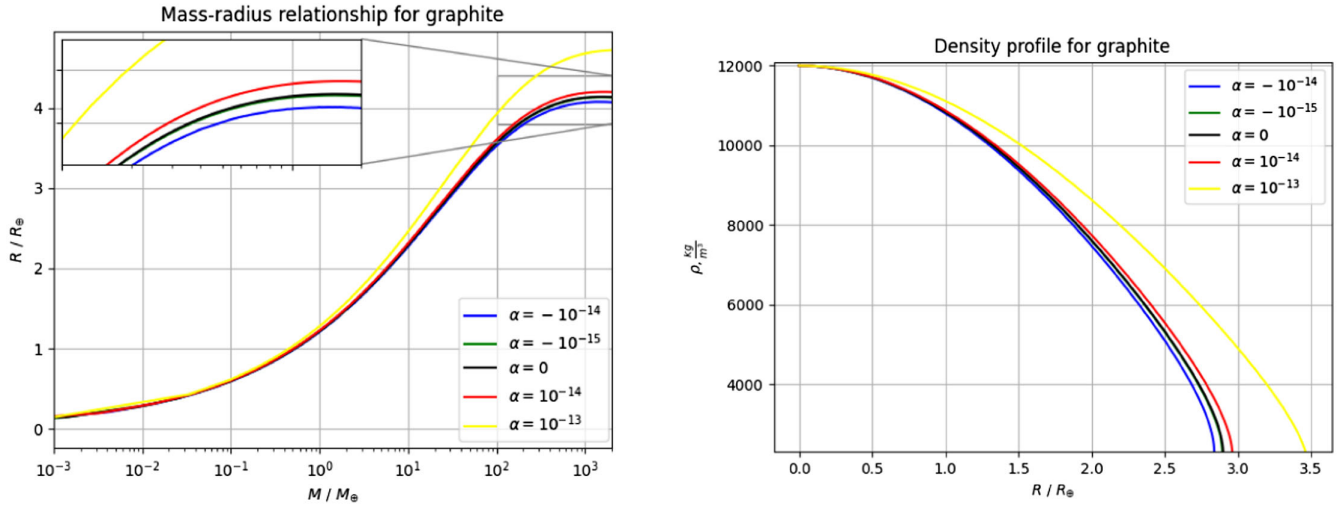

FIG. 9. Mass-radius relation and density profile plots for homogeneous cold spheres of graphite for different values of the parameter α (where $\alpha = 0$ gives a GR/Newtonian planet), obtained from the SKHM equation of state with the use of the modified hydrostatic equilibrium equations.

curves when compared to those obtained with the use of Newtonian equations. We also suspect that the layers' thickness will be influenced by a gravity model applied when more realistic internal structure is used—that is, when one takes into account the different layer structures of a given planet. These facts will also have an influence on the polar moment of inertia [Eq. (31)], giving a different result for each model of gravity.

On the other hand, a normalized polar planet's moment of inertia $\mathcal{C}/MR^2$ (where M is the planet's mass) is a quantity which can be obtained from the relation for the precession rate $d\psi/dt$ being caused by gravitational torques from the Sun [104]:

$$\frac{d\psi}{dt} = -\frac{3}{2} J_2 \cos\epsilon (1-e^2) \frac{n^2}{\omega} \frac{MR^2}{\mathcal{C}}, \tag{32}$$

where e is the orbital eccentricity, ϵ is the obliquity, ω is the rotation rate, and n is the effective mean motion, while $J_2 MR^2$ is a factor consisting of the principal moments of inertia (see, e.g., Refs. [105,106]; J_2 is the gravitational harmonic coefficient). This factor, as well as the other mentioned quantities, is well known in the case of the Solar System planets with high accuracy—in particular, for the Earth [107], as well as for Mars from the Viking [108,109], Mars Pathfinder [110], and other missions. So far, the opposite procedure has been applied in order to get to know the internal structure of a planet, as, for instance, in the cases of Mercury [111–116] and Venus [117–119]: from the many proposed density profiles and structural models, only those survive which give a moment of inertia [Eq. (31)] compatible with the one provided by the accurate observational data [Eq. (32)].

In what follows, we propose a procedure which allows us to constrain models of gravity using the already available seismic data of the Earth, and of Mars, when SEIS data obtained from analyzing waves created by marsquakes, thumps of meteorite impacts, surface vibrations generated by activity in Mars' atmosphere, and by weather phenomena (e.g., dust storms [103]) are ready. Such obtained density profiles in a given model of gravity, although sometimes carrying uncertainties regarding the most internal layers (the core), can be used to compute the polar moment of inertia [Eq. (31)], which must agree with the high accurate value acquired by observations [Eq. (32)]. Although Figs. 2 and 3 of the mass-radius relations do not demonstrate deviations from the Newtonian model in the case of the Earth and Mars, there are significant differences in the density profiles for the used values of the parameter α. It will affect the polar moment of inertia [Eq. (31)].

VI. DISCUSSION AND CONCLUSIONS

In this work, we have studied homogeneous cold spheres of low masses in the framework of Palatini $f(\mathcal{R})$ gravity. Those spheres are made of one of the six solid materials which are the most common substances found in the terrestrial planets. The mass-radius relations and density profiles obtained for each of the considered materials in our analysis have revealed that even for such low densities as the ones present in the rocky planets, modified gravity changes the curves, allowing us to draw interesting conclusions.

The mass-radius relation for homogeneous (and multiple layers' structure) spheres of various chemical compositions is an important tool providing an idea of the most abundant materials which an (exo)planet consists of, when its mass and radius are known, mainly from the observations of transiting exoplanets. Although such observations

can carry quite big uncertainties in the mass/radius ratios, once discovered, more powerful telescopes can follow up with new exoplanets to get more precise data. Furthermore, we are living in a very exciting epoch—more and more current and future scientific missions, such as, for instance, the current Cosmic Vision 2015–2025 (with a special focus on Cheops, Plato, Ariel, and Jupiter Icy Moons Explorer) [120] with further extensions of Voyage 2050 [121] from ESA, or the James Webb Space Telescope [122], Nancy Grace Roman Space Telescope [123], the Transiting Exoplanet Survey Satellite [124], Spitzer Space Telescope [125], and NN Explore [126] from NASA, are/will be collecting data on the Solar System planets and from other stars' systems.

Apart from the findings in regard to (exo)planets discussed in more detail below, we have also examined carefully a possible singular behavior of our equations, caused by the extra terms derived from the Palatini quadratic model (especially the one related to the conformal transformation [24,67]). More precisely, an eventual ill behavior of the hydrostatic equilibrium equations in Eq. (19), leading to nonphysical behavior of a spherical-symmetric system such as a planet or a star, could appear for a certain value of the parameter α. This particular value, as we observe from the relation in Eq. (27), is related to an equation of state. This is the reason why one needs to be careful when choosing the range of the parameter α (in the negative values' part) such that the considered EOS will not produce those values.

In conclusion, our results can be summarized by the following three main points:

(1) *Extra degeneracy in the mass-radius relation*.—Apart from the well-known degeneracy in the mass-radius relation, making the determination of the number of layers and their properties problematic already in a GR/Newtonian model [79], modified gravity introduces another one, caused by the additional theory parameter. Therefore, a transiting exoplanet may have slightly different layer structures and compositions for each of the layers than the ones predicted by the GR/Newtonian model, especially in the cases of carbon, water, and silicate planets (see the next point). Moreover, since iron is the most dense element out of which a planet can form, exoplanets with radii smaller than pure iron planets are not expected to be found. This limit is also well known, but as we can see in Fig. 4, modified gravity may shift the curves in the smaller-radius region. Finding more exoplanets of Mercury's type with very small radii [127] could be an additional indication that models other than general relativity and its Newtonian limit may have something to say in planetary physics.

(2) *Exoplanet properties*.—There are a few interesting properties one can determine about a type of transiting exoplanets when their masses and radii are known—the smaller the uncertainties in the mass and radius estimations,[4] the more characteristics of the exoplanet can be given. For example, as demonstrated in Ref. [79], planets above the water-ice curve must be richly abundant in the hydrogen and helium in their envelope; therefore, super-Earth exoplanets do not possess significant gas envelopes. As shown in Fig. 5, modified gravity may alter this conclusion a bit, since the large planets which are believed to have a considerable amount of those light elements in their atmospheres could be very poorly equipped in them in the case of theories of gravity other than GR/Newtonian.

Moreover, modified gravity can also shed light on some of the already existing hypotheses and problems related to planetary physics—such as, for example, planet migration and our knowledge of planetary system formation. Planets of certain structures and compositions are expected to be found at a particular distance from their host stars. Water planets (i.e., planets with more than 25% water ice by mass) can be identified with up to 5% fractional uncertainty in mass and radius, and they tend to have large radii [128]. They are usually found far from their host stars, and that fact, together with the current model of planetary system formation, is one of the leading points standing behind the idea of planet migration if water planets are found in a closer orbit. Therefore, one rather expects to detect a water exoplanet at the edge of a certain host star's system, while Earth-like planets, with the silicate main contribution, are supposed to be found at much smaller distances. This proposition is derived from the special position of the water-ice curve on the mass-radius plots, being an important hint for distinguishing rocky exoplanets from water ones and those with atmospheres rich in helium and hydrogen. However, as already marked out in the previous point, the water-ice curve is shifted in modified gravity. The (exo)planets lying close to the GR/Newtonian water curve may in reality still besolid planets, much less abundant in water, and not possessing envelopes rich in the light elements.

(3) *Constraining models using seismic data from the Earth and Mars*.—The significant difference in the density profiles of Figs. 4–9 between GR/Newtonian models and those provided by modified gravity, even for low-mass planets (Figs. 2 and 3), gives us an excellent opportunity to test and to constrain the existing models of gravity with the use of the known Earth and near-future Mars

[4]These estimations are related to the host star's properties, which also depend on the theory of gravity; for more details, see Refs. [39,42].

internal structures. The physics of low pressures and temperatures (in the meaning of planetary regimes) is much better understood than the physics of stars and their compact and ultracompact remnants.[5] In Sec. V, we have described the procedure which, after improving our toy planet's models, will be used to constrain given models of gravity. The polar moments of inertia for the Solar System planets—in particular, the Earth and Mars—are known with high accuracy [Eq. (32)], allowing us to compare them with those obtained from seismic data and the model of gravity, and eventually to discard those that are inconsistent with the observed ones.

Let us notice that our studies predict significant differences in the layers' thicknesses even for small values of the parameter α. They are more noticeable in the case of the heavier elements. Consequently, we speculate that the innermost layers, such as cores and mantles, consisting of mainly iron and silicates, respectively, will vary more noticeably in modified gravity models in comparison to the current ones. However, in order to say more in regards to that topic, we need to improve our model, enriching it in multiple layers of different compositions as suggested by the PREM and other models, as a starting point. Subsequently, a more consistent approach will require a reexamination of the current Earth and Mars models using earthquake and marsquake data, together with modified structure equations. Therefore, when seismic data are used in order to obtain density profiles in a given model of gravity—that is, when we know well enough the materials composing the different layers of the planet, as well as the layers' thicknesses in the GR/Newtonian and the modified gravity models—we may use them to examine the deviations caused by various gravitational proposals. Such a procedure will enable us to constrain the modified gravity models with respect to the given accuracy.

Let us just mention, as a concluding remark to that point, that so far, only helioseismic data has been used to constrain modified gravity models [131,132].

The results presented here and followed by future investigations will provide an accurate test and constraints of models of gravity from our nearest playground: the Earth and Mars. Works regarding this topic are already under development and will be soon presented to the physics community.

[5]However, it is not free from issues such as convective processes, inner core description, and discontinuities between layers, to mention just a few of them [129,130].

ACKNOWLEDGMENTS

This work was supported by the EU through the European Regional Development Fund CoE Program No. TK133, "The Dark Side of the Universe." A. K. is a beneficiary of the Dora Plus Program, organized by the University of Tartu. The authors would like to thank María José Vera and Gerardo Tejada Saracho for enlightening discussions on seismology and Mars missions.

APPENDIX: STRUCTURAL EQUATIONS USED IN THE NUMERICAL ANALYSIS

For the SKHM (modifed polytropic) equation of state

$$\rho(p) = \rho_0 + c p^n, \tag{A1}$$

the Palatini hydrostatic equilibrium equation (28) used in the numerical analysis has the following form:

$$\frac{d\rho}{dr} = -\frac{G\mathcal{M}\rho\left(\frac{4\pi\alpha\rho^2 r^3}{\mathcal{M}(2\alpha\rho+1)^{1/2}}+1\right)}{r^2(2\alpha\rho+1)^{1/2}\left(1-\frac{2G\mathcal{M}}{c^2 r(2\alpha\rho+1)^{1/2}}\right)} \times \frac{1}{\left(\frac{\alpha G\mathcal{M}\rho\left(\frac{4\pi\alpha\rho^2 r^3}{\mathcal{M}(2\alpha\rho+1)^{1/2}}+1\right)}{r(2\alpha\rho+1)^{3/2}\left(1-\frac{2G\mathcal{M}}{c^2 r(2\alpha\rho+1)^{1/2}}\right)}+\frac{2\alpha c^2\rho}{2\alpha\rho+1}+\frac{\left(\frac{\rho-\rho_0}{c_p}\right)^{\frac{1}{n}-1}}{c_p n}\right)}, \tag{A2}$$

while the mass function is given by Eq. (25).

Let us notice that when we consider a nonrelativistic limit of the full relativistic equation (19), one performs the expansion around $\alpha = 0$. This procedure causes the sign change in the extra term related to the modification in the nonrelativistic equation, which for the EOS given above takes the form

$$\frac{d\rho}{dr} \approx -\frac{Gm(r)\rho}{r^2}\frac{cn\left(\frac{\rho-\rho_0}{c}\right)^{\frac{n-1}{n}}(1-\alpha\rho)}{(1+2\alpha\frac{Gm}{r}cn\rho)\left(\frac{\rho-\rho_0}{c}\right)^{\frac{n-1}{n}}}. \tag{A3}$$

This is misleading and leads to the nonphysical behavior of the mass-radius and density curves in the case of large masses (large densities): in such a situation, the term $(1-\alpha\rho)$ may take negative values, changing the sign of the full expression (A3). It also suggests that a singular behavior of the equations would happen for positive values of the parameter α, but as we have already discussed in Sec. III B, an eventual singularity occurs for negative values. However, although we have not demonstrated it here, the nonrelativistic equation (A3) can be used for low-mass planets, with $M/M_{\text{Earth}} < 5$. In order to consider higher-mass (exo)planets as well, we have been using Eq. (A2), where we have simply skipped pressure terms in the combinations with energy density $\rho + p/c^2 \approx \rho$ and mass $pr^3/c^2\mathcal{M} \approx 0$, as its influence for the objects we study here is insignificant.

[1] C. M. Will, Living Rev. Relativity **17**, 4 (2014).
[2] B. P. Abbott *et al.* (LIGO Scientific and Virgo Collaborations), Phys. Rev. Lett. **119**, 161101 (2017).
[3] K. Akiyama *et al.* (Event Horizon Telescope Collaboration), Astrophys. J. **875**, L1 (2019).
[4] K. Akiyama *et al.* (Event Horizon Telescope Collaboration), Astrophys. J. Lett. **910**, L12 (2021).
[5] K. Akiyama *et al.* (Event Horizon Telescope Collaboration), Astrophys. J. Lett. **910**, L13 (2021).
[6] C. Goddi *et al.*, Astrophys. J. Lett. **910**, L14 (2021).
[7] L. Barack *et al.*, Classical Quantum Gravity **36**, 143001 (2019).
[8] E. J. Copeland, M. Sami, and S. Tsujikawa, Int. J. Mod. Phys. D **15**, 1753 (2006).
[9] S. Nojiri and S. D. Odintsov, Int. J. Geom. Methods Mod. Phys. **04**, 115 (2007).
[10] S. Nojiri, S. D. Odintsov, and V. K. Oikonomou, Phys. Rep. **692**, 1 (2017).
[11] S. Nojiri and S. D. Odintsov, Phys. Rep. **505**, 59 (2011).
[12] S. Capozziello and M. Francaviglia, Gen. Relativ. Gravit. **40**, 357 (2008).
[13] S. M. Carroll, A. De Felice, V. Duvvuri, D. A. Easson, M. Trodden, and M. S. Turner, Phys. Rev. D **71**, 063513 (2005).
[14] J. M. M. Senovilla and D. Garfinkle, Classical Quantum Gravity **32**, 124008 (2015).
[15] L. Parker and D. J. Toms, *Quantum Field Theory in Curved Spacetime: Quantized Fields and Gravity* (Cambridge University Press, Cambridge, England, 2009).
[16] N. D. Birrel and P. C. W. Davies, *Quantum Fields in Curved Space* (Cambridge University Press, Cambridge, England, 1982).
[17] M. Linares, T. Shahbaz, and J. Casares, Astrophys. J. **859**, 54 (2018).
[18] J. Antoniadis *et al.*, Science **340**, 6131 (2012).
[19] F. Crawford, M. S. E. Roberts, J. W. T. Hessels, S. M. Ransom, M. Livingstone, C. R. Tam, and V. M. Kaspi, Astrophys. J. **652**, 1499 (2006).
[20] R. Abbott *et al.*, Astrophys. J. **896**, L44 (2020).
[21] R. Abbott *et al.* (LIGO Scientific and Virgo Collaborations), Phys. Rev. Lett. **125**, 101102 (2020).
[22] J. Sakstein, Djuna Croon, Samuel D. McDermott, Maria C. Straight, and Eric J. Baxter, Phys. Rev. Lett. **125**, 261105 (2020).
[23] R. Saito, D. Yamauchi, S. Mizuno, J. Gleyzes, and D. Langlois, J. Cosmol. Astropart. Phys. 06 (2015) 008.
[24] A. Kozak and A. Wojnar, Eur. Phys. J. C **81**, 492 (2021).
[25] G. J. Olmo, D. Rubiera-García, and A. Wojnar, Phys. Rev. D **104**, 024045 (2021).
[26] G. J. Olmo, D. Rubiera-García, and A. Wojnar, Phys. Rep. **876**, 1 (2020).
[27] E. N. Saridakis *et al.* (CANTATA Collaboration), arXiv:2105.12582.
[28] S. Chandrasekhar, Mon. Not. R. Astron. Soc. **95**, 207 (1935).
[29] I. D. Saltas, I. Sawicki, and I. Lopes, J. Cosmol. Astropart. Phys. 05 (2018) 028.
[30] R. K. Jain, C. Kouvaris, and N. G. Nielsen, Phys. Rev. Lett. **116**, 151103 (2016).
[31] S. Banerjee, S. Shankar, and T. P. Singh, J. Cosmol. Astropart. Phys. 10 (2017) 004.
[32] A. Wojnar, Int. J. Geom. Methods Mod. Phys. **18**, 2140006 (2021).
[33] I. H. Belfaqih, H. Maulana, and A. Sulaksono, Int. J. Mod. Phys. D **30**, 2150064 (2021).
[34] J. Sakstein, Phys. Rev. Lett. **115**, 201101 (2015).
[35] J. Sakstein, Phys. Rev. D **92**, 124045 (2015).
[36] M. Crisostomi, M. Lewandowski, and F. Vernizzi, Phys. Rev. D **100**, 024025 (2019).
[37] G. J. Olmo, D. Rubiera-Garcia, and A. Wojnar, Phys. Rev. D **100**, 044020 (2019).
[38] A. S. Rosyadi, A. Sulaksono, H. A. Kassim, and N. Yusof, Eur. Phys. J. C **79**, 1030 (2019).
[39] A. Wojnar, Phys. Rev. D **102**, 124045 (2020).
[40] S. Chowdhury and T. Sarkar, J. Cosmol. Astropart. Phys. 05 (2021) 040.
[41] M. Benito and A. Wojnar, Phys. Rev. D **103**, 064032 (2021).
[42] A. Wojnar, Phys. Rev. D **103**, 044037 (2021).
[43] C. Brans and R. H. Dicke, Phys. Rev. **124**, 925 (1961).
[44] M. Andrews, Y.-Z. Chu, and M. Trodden, Phys. Rev. D **88**, 084028 (2013).
[45] L. Iorio, J. Cosmol. Astropart. Phys. 07 (2012) 001.
[46] T. Harko, Phys. Lett. B **669**, 376 (2008).
[47] H. Ozer and O. Delice, Classical Quantum Gravity **35**, 065002 (2018).
[48] S. Baghram, M. Farhang, and S. Rahvar, Phys. Rev. D **75**, 044024 (2007).
[49] S. Bahamonde, K. Flathmann, and C. Pfeifer, Phys. Rev. D **100**, 084064 (2019).
[50] H. J. Schmidt, Phys. Rev. D **78**, 023512 (2008).
[51] T. Harko, F. S. N. Lobo, S. Nojiri, and S. D. Odintsov, Phys. Rev. D **84**, 024020 (2011).
[52] L. Iorio, Adv. High Energy Phys. **2007**, 90731 (2007).
[53] A. Bonino, S. Camera, L. Fatibene, and A. Orizzonte, Eur. Phys. J. Plus **135**, 951 (2020).
[54] S. Bhattacharya and S. Chakraborty, Phys. Rev. D **95**, 044037 (2017).
[55] L. Iorio and M. L. Ruggiero, Open Astron. J. **3**, 167 (2010).
[56] M. Vargas dos Santos and D. F. Mota, Phys. Lett. B **769**, 485 (2017).
[57] J. D. Toniato, D. C. Rodrigues, and A. Wojnar, Phys. Rev. D **101**, 064050 (2020).
[58] P. K. Schwartz and D. Giulini, Phys. Rev. A **100**, 052116 (2019).
[59] G. J. Olmo, Phys. Rev. D **77**, 084021 (2008).
[60] G. J. Olmo, Phys. Rev. Lett. **98**, 061101 (2007).
[61] A. De Felice and S. Tsujikawa, Living Rev. Relativity **13**, 3 (2010).
[62] A. Stachowski, M. Szydlowski, and A. Borowiec, Eur. Phys. J. C **77**, 406 (2017).
[63] M. Szydlowski, A. Stachowski, and A. Borowiec, Eur. Phys. J. C **77**, 603 (2017).
[64] V. I. Afonso, G. J. Olmo, and D. Rubiera-Garcia, Phys. Rev. D **97**, 021503 (2018).
[65] V. I. Afonso, G. J. Olmo, E. Orazi, and D. Rubiera-Garcia, Eur. Phys. J. C **78**, 866 (2018).

[66] V. I. Afonso, G. J. Olmo, E. Orazi, and D. Rubiera-Garcia, Phys. Rev. D **99**, 044040 (2019).
[67] A. Wojnar, Eur. Phys. J. C **79**, 51 (2019).
[68] A. Wojnar, Eur. Phys. J. C **78**, 421 (2018).
[69] A. Borowiec and A. Kozak, J. Cosmol. Astropart. Phys. 07 (2020) 003.
[70] A. Kozak and A. Borowiec, Eur. Phys. J. C **79**, 335 (2019).
[71] L. Järv, P. Kuusk, M. Saal, and O. Vilson, Classical Quantum Gravity **32**, 235013 (2015).
[72] L. Järv, P. Kuusk, M. Saal, and O. Vilson, Phys. Rev. D **91**, 024041 (2015).
[73] P. Kuusk, M. Runkla, M. Saal, and O. Vilson, Classical Quantum Gravity **33**, 195008 (2016).
[74] A. Karam, T. Pappas, and K. Tamvakis, Phys. Rev. D **96**, 064036 (2017).
[75] A. Karam, A. Lykkas, and K. Tamvakis, Phys. Rev. D **97**, 124036 (2018).
[76] S. P. Weppner, J. P. McKelvey, K. D. Thielen, and A. K. Zielinski, Mon. Not. R. Astron. Soc. **452**, 1375 (2015).
[77] F. Birch, Phys. Rev. **71**, 809 (1947).
[78] J.-P. Poirier, *Introduction to the Physics of the Earth's Interior* (Cambridge University Press, Cambridge, England, 2000).
[79] S. Seager, M. Kuchner, C. A. Hier-Majumder, and B. Militzer, Astrophys. J. **669**, 1279 (2007).
[80] L. H. Thomas, Proc. Cambridge Philos. Soc. **23**, 542 (1927).
[81] E. Fermi, Z. Phys. **48**, 73 (1928).
[82] P. A. M. Dirac, Math. Proc. Cambridge Philos. Soc. **26**, 376 (1930).
[83] R. P. Feynman, S. Metropolis, and E. Teller, Phys. Rev. **75**, 1561 (1949).
[84] E. E. Salpeter and H. S. Zapolsky, Phys. Rev. **158**, 876 (1967).
[85] A. V. Astashenok, S. D. Odintsov, and A. de la Cruz-Dombriz, Classical Quantum Gravity **34**, 205008 (2017).
[86] S. Weinberg, *Gravitation and Cosmology: Principles and Applications of the General Theory of Relativity* (John Wiley & Sons, Inc., Toronto, 1972).
[87] A. Ganguly, R. Gannouji, R. Goswami, and S. Ray, Phys. Rev. D **89**, 064019 (2014).
[88] G. J. Olmo, Phys. Rev. D **78**, 104026 (2008).
[89] H-Ch. Kim, Phys. Rev. D **89**, 064001 (2014).
[90] T. Tsuchida, G. Kawamura, and K. Watanabe, Prog. Theor. Phys. **100**, 291 (1998).
[91] N. Dadhich and S. Chakraborty, Phys. Rev. D **95**, 064059 (2017).
[92] A. Wojnar, Acta Phys. Pol. B Proc. Suppl. **13**, 249 (2020).
[93] A. M. Dziewonski and D. L. Anderson, Phys. Earth Planet. Inter. **25**, 297 (1981).
[94] H. S. Zapolsky and E. E. Salper, Astrophys. J. **158**, 809 (1969).
[95] B. Brugger, J. Lunine, O Mousis, and M. Deleuil, EPSC Abstracts **13**, EPSC-DPS2019-983-1 (2019), https://meetingorganizer.copernicus.org/EPSC-DPS2019/EPSC-DPS2019-983-1.pdf.
[96] NASA exoplanet archive, https://exoplanetarchive.ipac.caltech.edu/, accessed 26.06.2021.
[97] B. Brugger, O. Mousis, M. Deleuil, and F. Deschamps, Astrophys. J. **850**, 93 (2017).
[98] E. Ago *et al.*, Planet. Space Sci. **2**, 1 (2021).
[99] B. Kustowski, G. Ekström, and A. M. Dziewoński, J. Geophys. Res. **113**, B06306 (2008).
[100] B. L. N. Kennett and E. R. Engdahl, Geophys. J. Int. **105**, 429 (1991).
[101] B. L. N. Kennett, E. R. Engdahl, and R. Buland, Geophys. J. Int. **122**, 108 (1995).
[102] https://ds.iris.edu/ds/products/emc-referencemodels/
[103] https://mars.nasa.gov/insight/spacecraft/instruments/seis/
[104] W. M. Kaula, *An Introduction to Planetary Physics: The Terrestrial Planets* (Wiley, New York, 1968).
[105] B. G. Bills, J. Geophys. Res. **104**, 30773 (1999).
[106] W. M. Folkner, C. F. Yoder, D. N. Yuan, E. M. Standish, and R. A. Preston, Science **278**, 1749 (1997).
[107] J. G. Williams, Astron. J. **108**, 711 (1994).
[108] A. S. Konopliv and W. L. Sjogren, Publication 95-3, Jet Propulsion Laboratory, California Institute of Technology, 1995.
[109] D. E. Smith, F. J. Lerch, R. S. Nerem, M. T. Zuber, G. B. Patel, S. K. Fricke, and F. G. Lemoine, J. Geophys. Res. **98**, 20871 (1993).
[110] W. M. Folkner, R. D. Kahn, R. A. Preston, C. F. Yoder, E. M. Standish, J. G. Williams, C. D. Edwards, R. W. Hellings, T. M. Eubanks, and B. G. Bills, J. Geophys. Res. **102**, 4057 (1997).
[111] J.-L. Margot, Stanton J. Peale, Sean C. Solomon, Steven A. Hauck, Frank D. Ghigo, Raymond F. Jurgens, Marie Yseboodt, Jon D. Giorgini, Sebastiano Padovan, and Donald B. Campbell, J. Geophys. Res. **117**, E00L09 (2012).
[112] B. Brugger *et al.*, in *Proceedings of the European Planetary Science Congress* (2018), EPSC2018-404.
[113] G. Steinbrugge, M. Dumberry, A. Rivoldini, G. Schubert, H. Cao, D. M. Schroeder, and K. M. Soderlund, Geophys. Res. Lett. **48**, e2020GL089895 (2021).
[114] H. Harder and G. Schubert, Icarus **151**, 118 (2001).
[115] T. Spohn, F. Sohl, K. Wieczerkowski, and V. Conzelmann, Planet. Space Sci. **49**, 1561 (2001).
[116] M. A. Riner, C. R. Bina, M. S. Robinson, and S. J. Desch, J. Geophys. Res. **113**, E08013 (2008).
[117] J.-L. Margot *et al.*, Nat. Astron. **5**, 676 (2021).
[118] A. S. Konopliv and C. F. Yoder, Geophys. Res. Lett. **23**, 1857 (1996).
[119] C. Dumoulin, G. Tobie, O. Verhoeven, P. Rosenblatt, and N. Rambaux, J. Geophys. Res. **122**, 1338 (2017).
[120] https://www.esa.int/Science_Exploration/Space_Science/ESA_s_Cosmic_Vision
[121] https://www.esa.int/Science_Exploration/Space_Science/Voyage_2050_sets_sail_ESA_chooses_future_science_mission_themes
[122] https://www.nasa.gov/mission_pages/webb/about/index.html
[123] https://www.nasa.gov/feature/goddard/2021/nasa-s-roman-mission-will-probe-galaxy-s-core-for-hot-jupiters-brown-dwarfs.
[124] https://heasarc.gsfc.nasa.gov/docs/tess/.
[125] https://www.spitzer.caltech.edu/.
[126] https://exoplanets.nasa.gov/exep/NNExplore/.
[127] T. Barclay *et al.*, Nature (London) **494**, 452 (2013).

[128] D. Valencia, D. D. Sasselov, and R. J. O'Connell, Astrophys. J. **665**, 1413 (2007).
[129] K. C. Condie, in *Plate Tectonics and Crustal Evolution*, 4th ed. (Butterworth-Heinemann, London, 1997), ISBN 0-7506-3386-7.
[130] S. Karato, *Deformation of Earth Materials: An Introduction to the Rheology of Solid Earth* (Cambridge University Press, Cambridge, England, 2008), ISBN 0-521-84404-5.
[131] J. Casanellas, Astrophys. J. **745**, 15 (2012).
[132] I. D. Saltas and I. Lopes, Phys. Rev. Lett. **123**, 091103 (2019).